https://doi.org/10.1016/j.ejmech.2017.09.066

Effect of mofezolac-galactose distance in conjugates targeting cyclooxygenase (COX)-1 and CNS GLUT-1 carrier

Maria Grazia Perrone[a], Paola Vitale[a], Savina Ferorelli[a], Angelina Boccarelli[b], Mauro Coluccia[a], Alessandra Pannunzio[a], Federica Campanella[a], Giuseppe Di Mauro[c], Carmela Bonaccorso[c], Cosimo G. Fortuna[c], Antonio Scilimati[a,*]

[a] Department of Pharmacy - Pharmaceutical Sciences, University of Bari "Aldo Moro", Via E. Orabona 4, 70125 Bari, Italy
[b] Department of Biomedical Sciences and Human Oncology, University of Bari "Aldo Moro", Piazza Giulio Cesare 11, 70124 Bari, Italy [c] Department of Chemical Science, University of Catania, Viale Andrea Doria 6, 95125 Catania, Italy

Keywords:
Cyclooxygenase-1 inhibition
Mofezolac
Galmof
Caco-2 cell line
GLUT-1
Molecular modeling

a b s t r a c t

Neuroinflammation is the earliest stage of several neurological and neurodegenerative diseases. In the case of neurodegenerative disorders, it takes place about 15e20 years before the appearance of specific neurodegenerative clinical symptoms. Constitutive microglial COX-1 is one of the pro-inflammatory players of the neuroinflammation. Novel compounds 3, 14 and 15 ($Galmof_0$, $Galmof_5$ and $Galmof_{11}$, respectively) were projected, and their synthetic methodologies developed, by linking by an ester bond, directly or through a C5 or C11 unit linker the highly selective COX-1 inhibitor mofezolac (COXs selectivity index > 6000) to galactose in order to obtain substances capable to cross blood-brain barrier (BBB) and control the CNS inflammatory response. 3, 14 and 15 (Galmofs) were prepared in good to fair yields. $Galmof_0$ (3) was found to be a selective COX-1 inhibitor (COX-1 IC_{50} ¼ 0.27 mM and COX-2 IC_{50} ¼ 3.1 mM, selectivity index ¼ 11.5), chemically and metabolically stable, and capable to cross Caco-2 cell monolayer, resembling BBB, probing that its transport is GLUT-1-mediated. Furthermore, $Galmof_0$ (3) powerfully inhibits PGE_2 release higher than mofezolac (1) in LPS-stimulated mouse BV2 microglial cell line, a worldwide recognized neuroinflammation model. In addition, Fingerprints for Ligands and Proteins (FLAP) was used to explain the different binding interactions of Galmofs with the COX-1 active site.

1. Introduction

Up to now, there is no worldwide shared protocol to treat the human neuroinflammatory syndrom. Its onset and progression diagnosis are not yet possible by any hospital available technique, but only through lately appearance of clinical symptoms of encephalon diseases [1,2]. Chronic neuroinflammation is tightly connected to brain degenerative processes [3], and it is considered the earliest step of several neurodegenerative disorders such as Alzheimer and Parkinson disease, amyotrophic lateral sclerosis, multiple sclerosis, traumatic brain injury, and HIV encephalitis [4]. It seems that it takes approximately fifteen-twenty years from perpetuating insults inducing chronic neuroinflammation and clinical symptoms appearance of dementia or other neurodegenerative disorders [5].

The lack of drugs to treat several diseases involving the central nervous system (CNS) also resides into the shield exerted by the blood brain barrier (BBB) matrix. BBB has a low permeability, and the development of drugs able to penetrate through its network is one of the challenges of all scientists involved in projecting medicines having active principle ingredients targeting the CNS diseases. A commonly used strategy to overcome this drawback consists to incorporate into the pharmacological active molecule a sugar moiety (i.e. glucose or galactose), in turn capable to "carry" the entire molecule into the CNS by the GLUT-1 carrier, which is located on the membrane of the endothelial cells.

GLUT-1 belongs to a family of homologous proteins GLUT-1-5, which differ in their tissue distribution and affinity for naturally occurring hexoses. GLUT-1 is present in erythrocytes, BBB and placenta and has a nanomolar affinity constant for D-glucose and D-galactose [6].

The choice of the hexose to be conjugated to the active

* Corresponding author.
E-mail address: antonio.scilimati@uniba.it (A. Scilimati).

pharmaceutical ingredient (API) is based upon its involvement into the metabolic homeostasis [7]. D-Galactose has been preferred to D-glucose because the latter is involved in many metabolic activities, alterable by chronic administration of glucosyl derivatives. Furthermore, mofezolac was selected as API, being a highly selective cyclooxygenase(COX)-1 inhibitor [8]. It is commercially available in Japan as Disopain® and is clinically used to treat human algesia and rheumatoid arthritis.

Microglial COX-1 exerts its pro-neuroinflammatory role, by producing also the pro-inflammatory prostaglandin PGE_2 as a rapid response to several CNS inciting harmful stimuli. Thus, a selective COX-1 inhibition is expected to contribute to reduce neuroinflammation by blocking part of the complex network involved in the onset of the inflammatory process [9,10]. This prominent role of COX-1 over COX-2, the other known COX isoform, could be explained by considering that COX-1 is constitutively expressed in microglia, then the first response to inflammatory inducers is COX-1 mediated, whereas the second response is due to the induced COX-2 [4,5].

Hence, keeping on our work aimed at designing molecules capable to fit well into the COX-1 active site [11e14] and in this case also able to cross BBB, we projected the new molecules 3, 14e15 ($Galmof_0$, $Galmof_5$ and $Galmof_{11}$) in which mofezolac is directly linked to D-galactose or by linkers of different features. Herein, we report mofezolac synthesis optimization and the preparation of $Galmof_0$, $Galmof_5$ and $Galmof_{11}$. Their permeability across the monolayer of the human colon adenoma derived cell line (Caco-2) was also measured. Caco-2 cells were chosen as a model of BBB [15] crossing mediated by GLUT-1. Immunofluorescence experiments were performed to confirm the GLUT-1 expression in Caco-2 cell line and its involvement in the transport of 3, 14e15 through Caco-2 cell compact layer. Both chemical and metabolic stability of 3, resulting more potent and selective COX-1 inhibitor than 14 and 15, were evaluated. 3 was also evaluated, in comparison to mofezolac used as reference, in LPS-stimulated mouse BV2 microglial cell line, in turn is scientifically considered an in vitro model of neuroinflammation. Fingers for Ligands and Proteins (FLAP) software was used to rationalize the different COXs inhibition capability of the new synthesized compounds with respect to mofezolac, through the binding interactions between 3, 14e15 and COX-1 active site amino acids residues.

2. Results and discussion

3,14e15 ($Galmof_0$, $Galmof_5$ and $Galmof_{11}$, respectively) chemical structures were designed considering the Barnett's investigation [16], probing the importance of the hydroxyl at both D-glucose C1 and C3 as hydrogen-bonding acceptors during D-glucose crossing human erythrocyte sugar-transport system, presumably GLUT-1 [17]. Glucose C4-hydroxyl also binds GLUT-1 through a further H-bonding. In fact, D-galactose, as C4 epimer of D-glucose, has an affinity for GLUT-1 10-fold lower than D-glucose, that in turn could be explained by considering that the non-gluco configuration of the sugar hydroxyl group sterically hinders the transport [17]. The OH group at sugar-C6 seems to be not involved in H-bond with GLUT-1, and bulky substitutions (O-Alkyl or O-Phenyl) at this position are tolerated, whereas the same substitutions at the anomeric C1 are not tolerated [16]. Based on this GLUT-1 cell biology knowledge, 3, 14 and 15 were designed linking mofezolac to the galactose through its C6 hydroxyl group.

2.1. Synthesis of 3, 14e15 ($Galmof_0$, $Galmof_5$ and $Galmof_{11}$)

Mofezolac 1 was firstly esterified with 1,2:3,4-di-O-isopropylidene-a-D-galactopyranose (DIPG) in the presence of N-ethyl-N'-(3-dimethylaminopropyl)carbodiimide hydrochloride (EDC) and 4-(dimethylamino)pyridine (DMAP) to afford 1,2:3,4-di-O-isopropylidene-6-O-{2-[3,4-bis(4-methoxyphenyl)isoxazol-5-yl] acetyl}-D-galactopyranose (2), in turn deprotected with trifluoroacetic acid (TFA) to 3 ($Galmof_0$) (Scheme 1).

To prepare 14 ($Galmof_5$) and 15 ($Galmof_{11}$), mofezolac was linked to galactose by 5-aminopentanoic acid (4) or 11-aminoundecanoic acid (5), respectively. The acids 4 and 5 were first transformed into their corresponding methyl esters 6 and 7 in quantitative yields by $SOCl_2$/MeOH and then allowed to react with mofezolac 1 in the presence of 1-hydroxybenzotriazole hydrate (HOBt), dicyclohexylcarbodiimide (DCC) and N,N-diisopropylethylamine (DIEA) at r.t. to afford 8 and 9, respectively. Methyl esters 8 and 9 were, then, hydrolyzed to their corresponding acids 10 and 11 by LiOH/THF-H_2O, in turn reacted with DIPG to give 12 and 13, that were deprotected with TFA to 14 ($Galmof_5$) and 15 ($Galmof_{11}$) (Scheme 2).

2.2. Immunofluorescence experiments

Caco-2 cell monolayer is a commonly used in vitro method to predict a compound ability to permeate physiological barriers [18]. The presence of GLUT-1 in Caco-2 cells was verified by immunofluorescence experiments before testing whether the biological membrane crossing by the newly synthesized compounds is carrier-mediated. Caco-2 cells were fixed and immunofluorescently stained with an anti-GLUT-1 mouse monoclonal antibody. The primary antibody was visualized using AlexaFluor® 594 labeled secondary antibody and the nuclei were counterstained with Hoechst 33342. There was a positive GLUT-1 signal staining in the cells incubated with anti-GLUT-1 mouse monoclonal antibody, whereas no staining was observed in the cells incubated with BSA 3% (no immune control) (Fig. 1).

2.3. Permeability experiments by 3, 14 and 15 (Galmofs)

Once the presence of GLUT-1 in Caco-2 cells was confirmed [19], the newly synthesized compounds 3, 14 and 15 ($Galmof_0$, $Galmof_5$ and $Galmof_{11}$) were assayed for their ability to permeate the compact layer of Caco-2 cells expressing GLUT-1 (Fig. 2).

The Apparent Permeability (Papp) in both basolateral to apical [Papp(B/A)] and apical to basolateral [Papp(A/B)] directions was determined. The [Papp(B/A)] flux of each compound alone or in the presence of phloretin, a GLUT-1 inhibitor, was determined (Table 1). (B/A) flux represents the active transport since GLUT-1 is expressed in the basolateral compartment [19]. Then, a high (B/A) flux value would mean that the transport might be GLUT-1 mediated (Fig. 2). The (A/B) flux, representing the passive transport, was also been determined for each compound (Table 1).

(B/A) and (A/B) fluxes of 1 (mofezolac) were also determined. The corresponding Papp values were found to be comparable since no active transport is involved, probably due to the absence in the molecule of a sugar moiety that would be recognized by GLUT-1. Higher Papp (B/A) values than 1 (mofezolac) were observed for all Galmofs, indicating that a carrier-mediated active transport mechanism is implicated. 3 ($Galmof_0$) shows an apparent permeability of 875 nm/s, whereas in the presence of phloretin, a 30% reduction of the basolateral to apical flux was observed [Papp (B/A) ¼ 610 nm/s], and the passive transport is not affected by GLUT-1 inhibitor pre-treatment. For 14 ($Galmof_5$) the percentage of the apparent permeability reduction is of 32%, similarly to 3 ($Galmof_0$); [Papp (B/A)] varies from 1129 to 771 nm/s in the presence of the GLUT-1 inhibitor. The apparent permeability of 15 ($Galmof_{11}$) [Papp (B/A) ¼ 587 nm/s] in the presence of phloretin decreases by 30% [Papp (B/A) ¼ 415 nm/s].14 and 15 passive transport remains

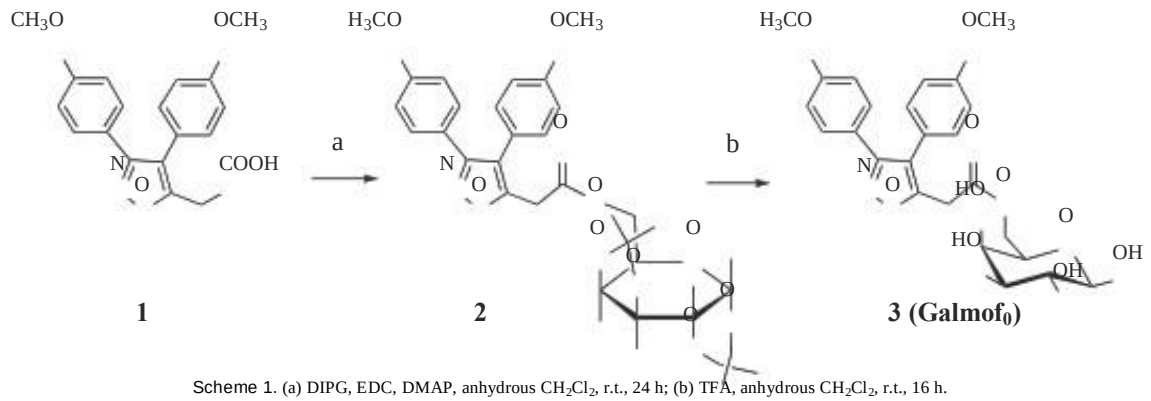

Scheme 1. (a) DIPG, EDC, DMAP, anhydrous CH_2Cl_2, r.t., 24 h; (b) TFA, anhydrous CH_2Cl_2, r.t., 16 h.

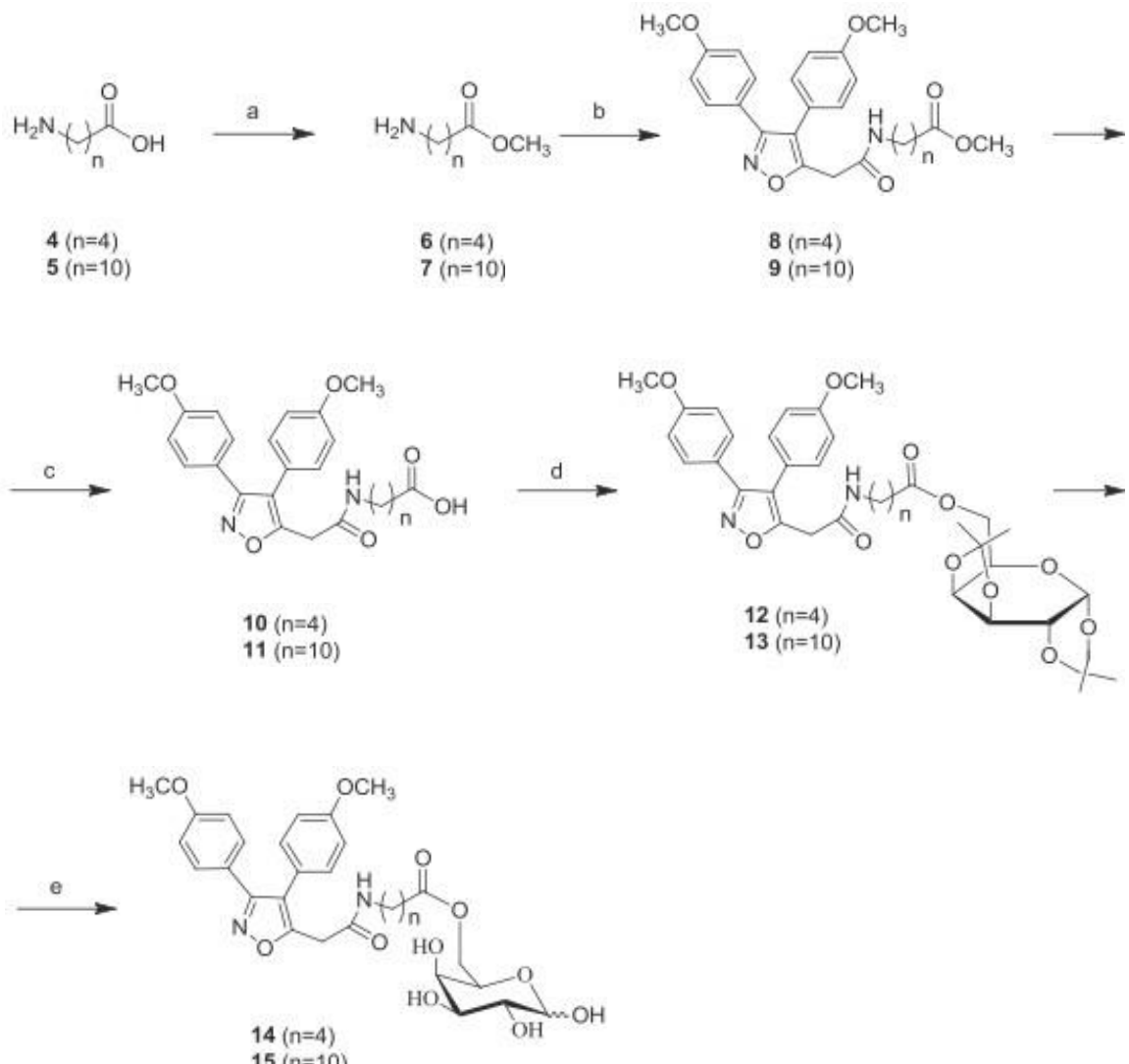

Scheme 2. (a) $SOCl_2$, anhydrous MeOH; (b) mofezolac 1, HOBt, DCC, DIEA, anhydrous CH_2Cl_2, r.t., 24 h; (c) LiOH/THF-H_2O, 3 h, HCl; (d) DIPG, EDC, DMAP, anhydrous CH_2Cl_2, r.t., 24 h; (e) TFA, anhydrous CH_2Cl_2, r.t., 16 h.

unchanged independently from the phloretin pre-incubation (Table 1).

These flux extent reductions, in the presence of phloretin (approximately 30%), indirectly demonstrate the involvement of GLUT-1 in Galmofs transport across the monolayer of Caco-2 cells.

Overall, it can be assumed that when mofezolac is linked to galactose (3, 14e15) is capable to cross the cell monolayer faster than mofezolac alone. In fact, 1 [Papp (B/A)] ¼ 461 nm/s becomes 875, 1129 and 587 nm/s for 3 ($Galmof_0$), 14 ($Galmof_5$) and 15 ($Galmof_{11}$), respectively. These data were confirmed by

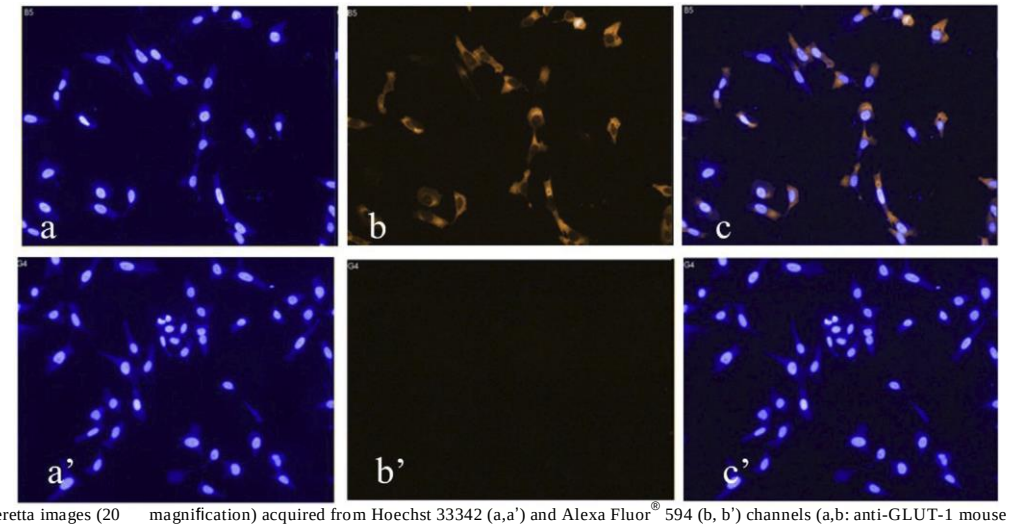

Fig. 1. Perkin-Elmer Operetta images (20 magnification) acquired from Hoechst 33342 (a,a') and Alexa Fluor® 594 (b, b') channels (a,b: anti-GLUT-1 mouse monoclonal antibody; a',b': no immune control). Merged images of a-b ad a'-b' are shown in c and c', respectively.

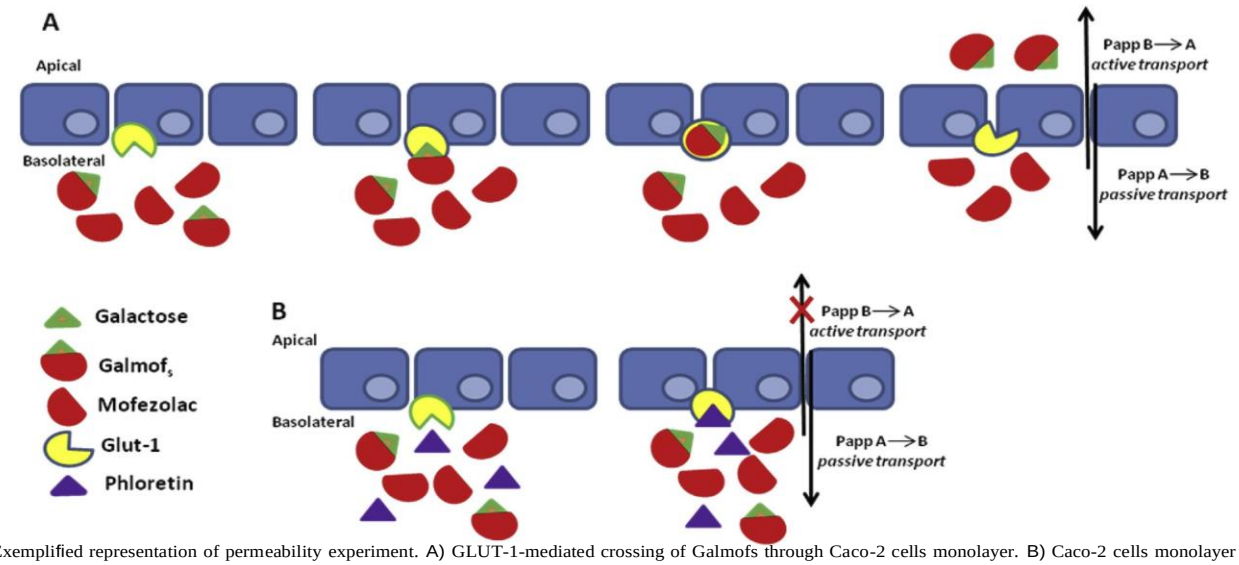

Fig. 2. Exemplified representation of permeability experiment. A) GLUT-1-mediated crossing of Galmofs through Caco-2 cells monolayer. B) Caco-2 cells monolayer crossing by Galmofs prevented by the GLUT-1 inhibitor phloretin.

Table 1
Papp (nm/sec) values of 3,14e15 ($Galmof_0$, $Galmof_5$ and $Galmof_{11}$) alone or in the presence of 100 mM phloretin.

Compounds	Papp B/A (nm/sec)		Papp A/B (nm/sec)	
1	461		414	
		phloretin		phloretin
3	875	610[a]	380	368[a]
14	1129	771[a]	233	289[a]
15	587	415[a]	169	172[a]

[a] Papp was determined after 24 h incubation of cells with 100 mM phloretin (GLUT-1 inhibitor).

immunofluorescence and transportability experiments.

2.4. Fluorescence competition binding assay

Competitive 2-NBDG cell uptake assays were performed to further probe the involvement of GLUT-1 in the transport of the newly synthesized compounds 3, 14 and 15 in Caco-2 cell system. D-Glucose transport, the GLUT-1 natural substrate, was used as a reference. 2-NBDG is a fluorescently labeled deoxyglucose analogue primarily used to directly monitor glucose uptake through GLUTs, by living cells and tissues [20]. Specifically, Fig. 3 shows the competitive inhibition of 2-NBDG by D-glucose and the phloretin GLUT-1 inhibitor [21].

2-NBDG uptake in Caco-2 cells was found to be dose-dependent (see Supplementary material). Its uptake (Fig. 4A) and consequently the percentage of labeled cells (Fig. 4B) were reduced with increasing D-glucose concentrations (1, 5 and 10 mM). Similarly, increasing concentrations (0.01, 0.5 and 0.1 mM) of 3 ($Galmof_0$), 14 ($Galmof_5$), and 15 ($Galmof_{11}$) reduced 2-NBDG uptake, supporting the idea that their transport is GLUT-1-mediated (Fig. 4).

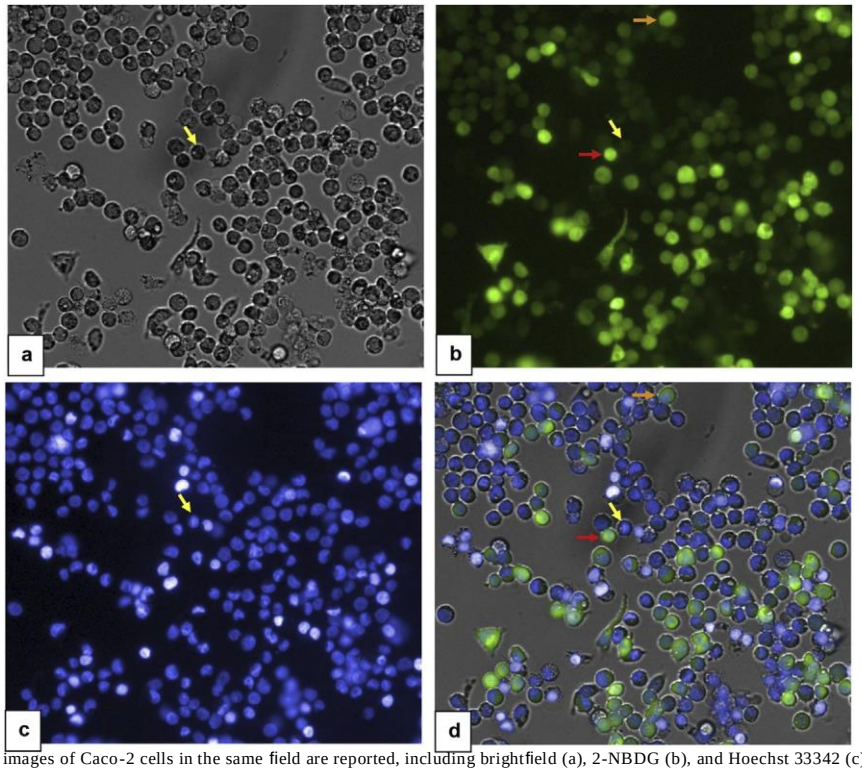

Fig. 3. Representative microscopic images of Caco-2 cells in the same field are reported, including brightfield (a), 2-NBDG (b), and Hoechst 33342 (c) channels, and colored overlay (d). Variability of 2-NBDG uptake by Caco-2 cells is shown through examples of i) cells with no 2-NBDG label, ii) diffusely 2-NBDG-labeled cells, and iii) cells with granular morphology pattern of 2-NBDG labeling, identified by yellow, red, and orange arrows, respectively. (For interpretation of the references to colour in this figure legend, the reader is referred to the web version of this article.)

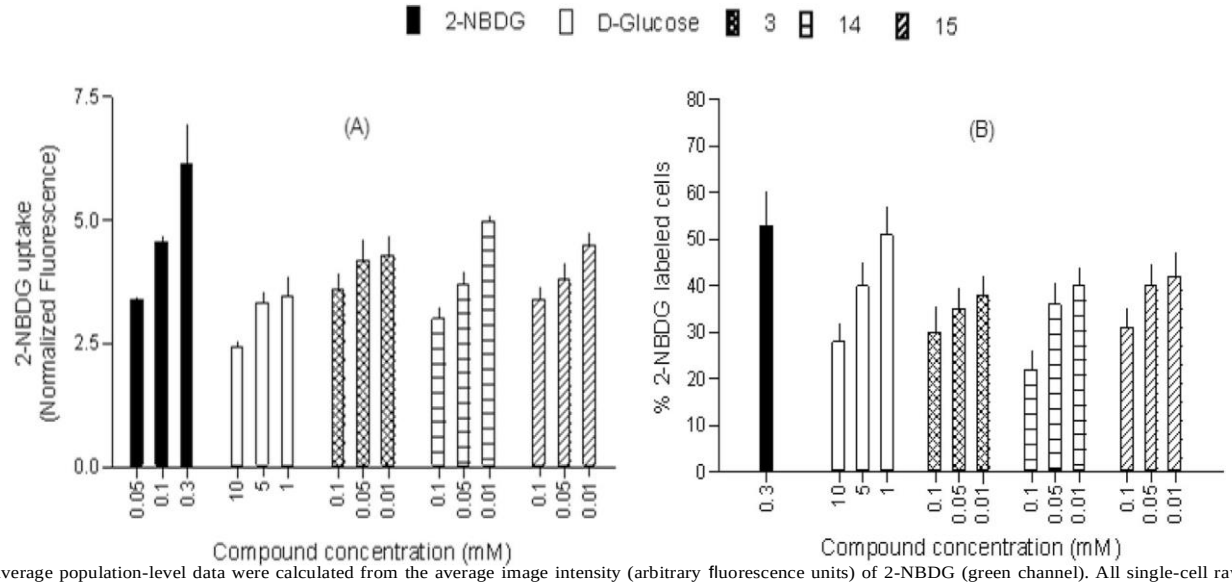

Fig. 4. Average population-level data were calculated from the average image intensity (arbitrary fluorescence units) of 2-NBDG (green channel). All single-cell raw data were normalized to background level, and presented as mean ± SEM of three independent experiments. (b) The percentage of 2-NBDG-labeled cells (on total cell number) for 2-NBDG (0.3 mM), Galmofs compounds (0.01e0.1 mM) and D-glucose (1e10 mM) is shown.

2.5. Cytofluorimetric analysis of Caco-2 cell cycle

Cytofluorimetric analysis of Caco-2 cell cycle was performed to evaluate the effects of mofezolac and Galmofs on cellular cycle of Caco-2 cells used for permeability and competition binding assays. The treatment of Caco-2 cells for 24 h with 100 mM of each compound (1, 3, 14e15) shows a common cytostatic effect. In particular, compound 14 ($Galmof_5$) has a prolonged and marked effect in phase S and G2/M. Conversely, compounds 3 ($Galmof_0$) and 15 ($Galmof_{11}$) show control over a cycle recovery that is more effective in compound 15 ($Galmof_{11}$) than compound 3 ($Galmof_0$) (Fig. 5). These results demonstrate that only compound 14

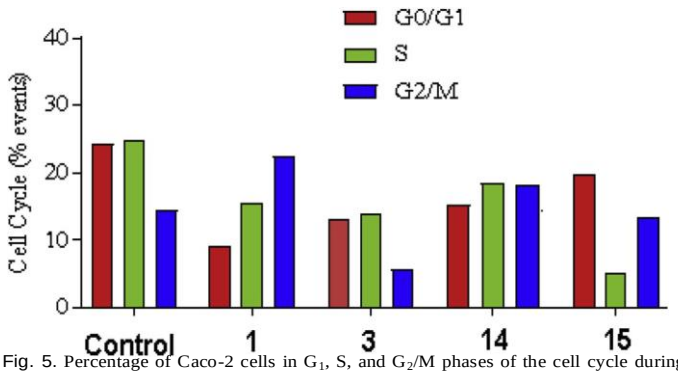

Fig. 5. Percentage of Caco-2 cells in G_1, S, and G_2/M phases of the cell cycle during continuous exposure to 1 (mofezolac), 3 ($Galmof_0$), 14 ($Galmof_5$), and 15 ($Galmof_{11}$) or control (untreated cells) for 24 h at the concentration of 100 mM.

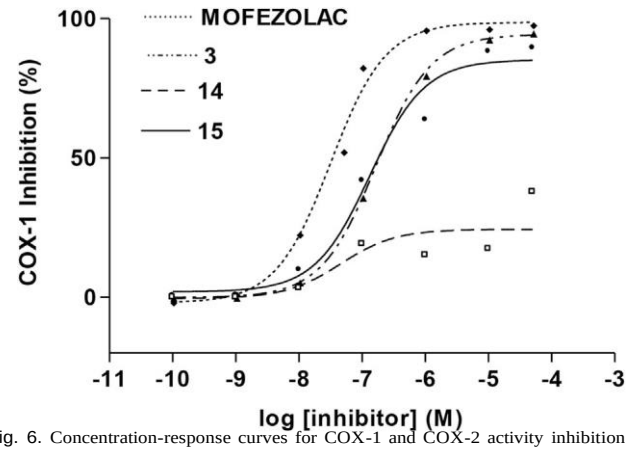

Fig. 6. Concentration-response curves for COX-1 and COX-2 activity inhibition by 1 (mofezolac) and 3, 14e15 ($Galmof_0$, $Galmof_5$ and $Galmof_{11}$, respectively).

($Galmof_5$) at the high dose of 100 mM perturbs the cell cycle, for all the other compounds only a transient alteration of the normal phases of the cycle was observed.

2.6. Cyclooxygenase inhibition evaluation

Human cyclooxygenase activity inhibition was determined by a colorimetric COX Inhibitor Screening Assay which measures the peroxidase component of the cyclooxygenases, monitoring the appearance of oxidized N,N,N^0,N^0-tetramethyl-p-phenylenediamine (TMPD) at l ¼ 590 nm. 1 (mofezolac) is a selective and potent COX-1 inhibitor with IC_{50} ¼ 0.0079 mM and 38% inhibition on COX-2 at the highest final inhibitor concentration of 50 mM. The conjugation of 1 with D-galactose (3) determines a reduction of potency and selectivity: COX-1 IC_{50} ¼ 0.27 mM and COX-2 IC_{50} ¼ 3.1 mM with 87% inhibition on COX-2 isoform at the highest final inhibitor concentration of 50 mM. The insertion of a C5-linker (8) between the two moieties 1 (mofezolac) and galactose was found to be detrimental to the COXs inhibitory activity of 14 ($Galmof_5$). In fact, its IC_{50} was higher than 50 mM for both isoforms and the inhibition percentages, at this concentration, were found to be 38% for COX-1 and 24% for COX-2. The presence of the longer spacer determined a recovery of COXs inhibition potency, infact 15 ($Galmof_{11}$) has a COX-1 IC_{50} ¼ 0.40 mM and 0.27 mM for COX-2, and an inhibition percentage of 90 and 64% for COX-1 and COX-2, respectively, at the highest final inhibitor concentration of 50 mM (Table 2 and Fig. 6) (see Fig. 7).

2.7. Effect of $Galmof_0$ 3 vs mofezolac 1 on PGE_2 biosynthesis in LPS-stimulated mouse BV2 microglial cells

The PGE_2 biosynthesis extent was evaluated in supernatants of cell cultures at 48 h incubation time (Table 3). PGE_2 production in LPS-stimulated cells was significantly higher than its basal level present in the untreated cells (control). Interestingly, both COX-1 inhibitors reduce PGE_2 release in LPS-treated cells (Table 3). Specifically, $Galmof_0$ was found to be more effective than mofezolac even at a higher concentration (10 mM for 3 vs 0.5 mM for 1) (Table 3), [10].

2.8. Modeling studies

The conjugation of mofezolac with D-galactose determined a change the inhibitory in potency and selectivity for all the three newly synthesized compounds with respect to 1. As an attempt to find out the rationale of such results, an in silico study of the binding mode of 3,14e15 ($Galmof_0$, $Galmof_5$ and $Galmof_{11}$) into the cavity of the target COX-1 co-crystallized with 1 (mofezolac) (PDB code: 5HQK) [8] was performed using the Fingerprints for Ligands and Proteins (FLAP) method [22].

2.9. Structure-based binding mode

FLAP is a Virtual-Screening and Model-Development method based on 3D molecular similarity that is measured through common Molecular Interaction Field (MIF) volumes generated by GRID. FLAP is an extremely flexible method that enables a wide variety of applications, from ligand-based Virtual-Screening [23e25] and 3D pharmacophore hypothesis generation [26,27], to structure-based Virtual-Screening [28] and high-throughput proteins pockets clustering. FLAP structure-based approach was used to investigate the possible binding modes of 3, and 14e15 (Galmofs) in COX-1 active site.

The X-ray structure of 1 (mofezolac) was removed from the COX-1:1 complex crystal structure [8], and the GRID [29] molecular interaction fields were computed into the cavity. To validate the

Table 2
COX inhibitory activity of 1 and 3, 14 and 15.

Compound	COX-1		COX-2		SI[c]
	IC_{50} (mM)[a]	inhibition (%)[b]	IC_{50} (mM)[a]	inhibition (%)[b]	
1	0.0079 ± 0.15	100	>50	38	6392
3	0.27 ± 0.09	100	3.1 ± 0.4	87	11.5
14	>50	38	>50	24	e
15	0.40 ± 0.05	90	0.27 ± 0.03	64	0.67

[a] IC_{50} values are the means of at least three independent measurements.
[b] Inhibition percentage (%) was determined at the highest final concentration of inhibitor used (50 mM). [c] SI (Selectivity Index) ¼ COX-2 IC_{50}/COX-1 IC_{50}.

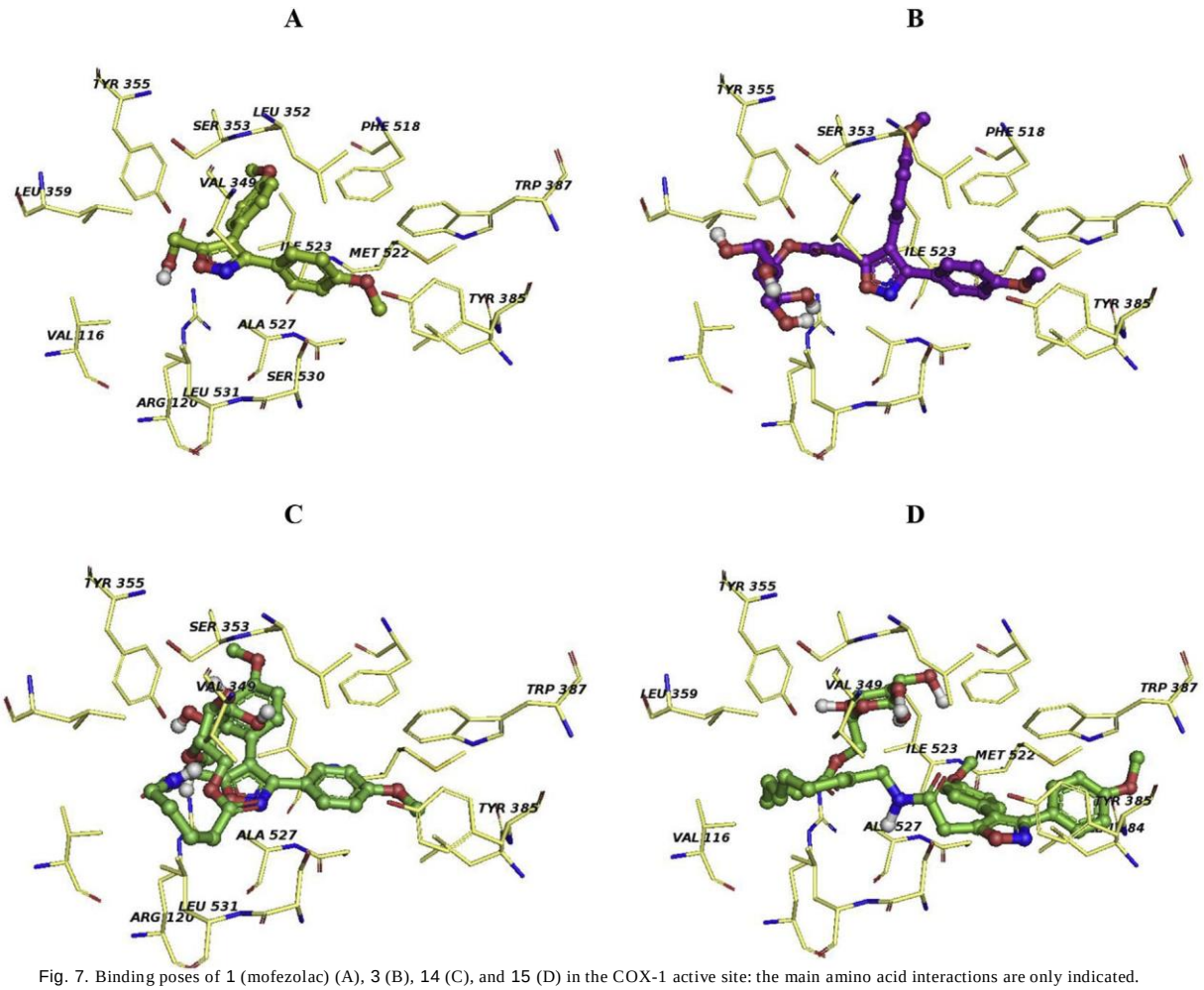

Fig. 7. Binding poses of 1 (mofezolac) (A), 3 (B), 14 (C), and 15 (D) in the COX-1 active site: the main amino acid interactions are only indicated.

Table 3
Effect of Galmof$_0$ 3 and mofezolac 1 on PGE_2 release (ng/ml) after 48 h in lipopolysaccharide (LPS)-stimulated mouse BV2 microglial cells.

Control	LPS	0.5 mM 3 þ LPS	1 mM 3 þ LPS	10 mM 3 þ LPS	0.5 mM 1 þ LPS
0.4540 ± 0.006	0.7555 ± 0.032	0.0086 ± 0.0002	0.0178 ± 0.0003	0.0103 ± 0.0006	0.0328 ± 0.002

model generated by FLAP, the binding pose of 1, without any constrain, was studied. Its binding pose in the COX-1 active site was found to be coincident with the pose of mofezolac in the above mentioned complex reported in PDB 5HQK (Supplementary material, Fig. 3.1) [8].

As far as 3 (Galmof$_0$) is concerned, most of the interactions of 1 (mofezolac) with COX-1 active site are retained. The methoxy group linked to the phenyl ring at isoxazole C3 interacts with Tyr385 whereas the methoxy of the phenyl ring in position C4 with Ser353, and hydrophobic interaction of the phenyl ring with Ile523 and Phe518 was observed. The presence of all the galactose polar groups would suggest the establishment of new interactions between 3 (Galmof$_0$) and the enzyme catalytic cavity, and from a comparison of the best poses of 3 and 1 (Supplementary material, Fig. 3.2) it is evident that, despite the presence of galactose moiety, the interactions of 1 moiety and the amino acid residues forming the cyclooxygenase-1 catalytic cavity are still predominant, so that the two molecules 3 and 1 fitting in COX-1 active site is almost the same.

Analyzing 14 (Galmof$_5$), and 15 (Galmof$_{11}$) best poses (Supplementary material, Fig. 3.3 and 3.4, respectively), it is, instead, clear that the presence of a spacer between 1 portion and galactose leads to a different disposition of the two compounds in the COX-1 active site.

In particular, for 14 the methoxy group of the phenyl ring at isoxazole C4 interacts with Ser353. The OH in position 2^0 of the galactose ring interacts with Tyr355, whereas the OH at position 1^0 interacts with Arg120. The phenyl ring at the isoxazole C3 shows a hydrophobic interaction with Ala527 and Trp387, and the methylenic chain presents a hydrophobic interaction with Leu531 and Val349. For compound 15, the isoxazole ring interacts with Tyr385 establishing a H-bond. The OH at 4^0 of the galactose interacts with Tyr355, and the methoxy group of the phenyl ring in position C4 interacts with Met522 and Ile523. A hydrophobic interaction was also observed with Leu384, Ala527, Met522 and Trp387. The methylenic chain shows a hydrophobic interaction with Val349, Leu359 and Val116.

The different binding interactions described-above and an

increase number of methylene in the spacers, which corresponds to a change in the pocket fitting, could explain the different in vitro COXs inhibitory activity values (Table 2 and Fig. 6). These results are corroborated by a statistic analysis of the scores reported in Table 4 and Fig. 8, where the available screening results are listed and depicted.

The GRID approach is a well assessed concept for determining energetically favorable interaction sites in molecules with known structure using chemical probes e.g., H, O, N1, and DRY probes which describes the shape, hydrogen bond acceptor, hydrogen bond donor and hydrophobic interactions, respectively. FLAP creates a common reference framework in two steps: first, the MIFs of the molecules are calculated using the GRID force fields, and the resulting MIF's are condensed in complexity by extracting points (quadruplets or hotspot) representing the most favorable interactions. Second, each quadruplet of these points is used to generate different superpositions of the test molecules onto a template molecule. The quadruplets of each molecule are stored as a pharmacophoric fingerprints and used to evaluate their similarity. Superimposition of quadruplets is assessed through Probe scores and Distance scores, which represents the degree of overlap of the MIFs for each probe individually as well as for their combinations and overall difference of probe score between the ligand and template, respectively. In addition, FLAP calculates Global Sum scores (Glob_Sum) and Global Product scores (Glob_Prod). The former score is produced by summing all the scores of the individual probes together and the later score is produced by multiplying all the scores of the individual probes together [26,27].

The distance parameter of the three Galmofs and mofezolac are comparable, which justifies the goodness of the developed model.

In particular, analyzing the Glob Sum (G.S.) value, which takes into account the sum of the interactions with all the probes, and the DRY values which are linkable to the different length of the spacers, it is possible to deduce a stronger binding interaction for 3 and 15 than 14, that could justify the differences in the in vitro COXs inhibitory activity values (Table 2). The analysis of all these statistic data could be useful for the modeling of a new molecule, eventually more potent than mofezolac, by designing a pharmacophore that indicates the retained features for an active scaffold.

2.10. In vitro chemical and metabolic stability of 3 (Galmof$_0$)

The chemical stability of 3 was determined in three different buffer simulating the gastric fluid (pH ¼ 1.0; 0.1 M HCl), blood and gut district (pH ¼ 7.3 and 8.8, respectively), whereas its metabolic stability was evaluated in rat liver S9 fraction. It is noteworthy that 3 remained unchanged in all the investigated conditions, and specifically 60 min for the chemical stability and 30 min for the metabolic stability.

3. Conclusion

In conclusion, with this work novel compounds named Galmofs (3, 14e15) were prepared in good to fair yields by linking 1 (mofezolac) and a galactose molecule with or without a spacer of different length. They were opportunely designed to allow mofezolac to cross BBB and exert its selective CNS COX-1 inhibition action. Modeling accomplished studies highlight the interactions between COX-1 active site and the Galmofs and justify the difference in potency and selectivity of the three novel compounds with respect to mofezolac. In particular, the lack (3) or presence (14e15) of a spacer with different length changes the orientation of the entire molecule within the COX-1 catalytic cavity due to new stronger interactions in the case of 3 and 15 than 14.

In particular, 3 (Galmof$_0$) was found to be a COX-1 inhibitor (COX-1 IC_{50} ¼ 0.27 mM and COX-2 IC_{50} ¼ 3.1 mM) with a selectivity index of 11.5, showing both a good chemical (pH ¼ 1.0, 7.3 and 8.0) and metabolic (rat liver S9 fraction) stability, resulting capable to cross Caco-2 cell monolayer. Moreover, in the neuroinflammation model of LPS-stimulated mouse BV2 microglial cell, Galmof$_0$ (3) powerfully inhibits PGE_2 release higher than mofezolac 1, thus demonstrating to be a good candidate for further investigations in neurological and neurodegenerative diseases with a marked inflammatory component.

Table 4
Scores for mofezolac (1) and 3, 14e15 (Galmof$_0$, Galmof$_5$, Galmof$_{11}$) in COX-1:mofezolac crystal structure determined by X-ray crystallography.

Compound	Distance	Glob Prod	Glob Sum	H	N1	Dry	O
1	8.820	0.560	2.108	0.955	0.146	1.106	0.314
3	8.534	0.725	2.150	0.907	0.083	1.325	0.498
14	8.026	0.626	2.087	0.878	0.266	1.107	0.426
15	9.053	0.543	2.015	0.259	0.259	1.322	0.367

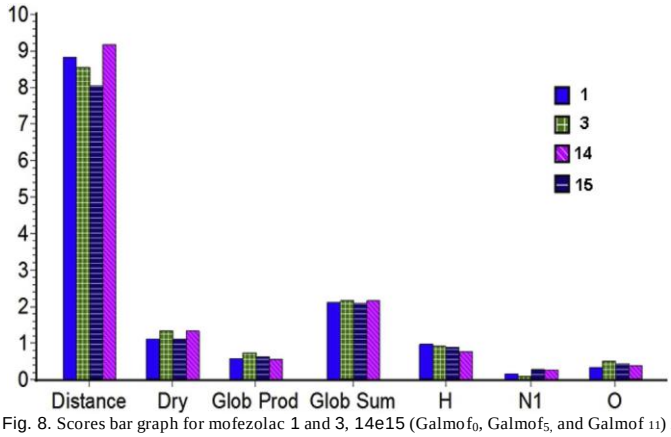

Fig. 8. Scores bar graph for mofezolac 1 and 3, 14e15 (Galmof$_0$, Galmof$_5$, and Galmof $_{11}$) in COX-1:mofezolac crystal.

4. Experimental section

4.1. Reagents and procedures - chemistry

Melting points taken on an Electrothermal apparatus were uncorrected. ^{1}H NMR and ^{13}C NMR spectra were recorded on a Varian-Mercury 300 MHz, Bruker-Aspect 3000 console 500 MHz spectrometer, or Bruker 600 MHz; chemical shifts are reported in parts per million (d). FT-IR spectra were recorded on a Perkin-Elmer 681 spectrometer. Thin-layer chromatography (TLC) was performed on silica gel sheets with fluorescent indicator. The spots on the TLC were visualized under ultraviolet light. Chromatography was conducted by using silica gel 60 with a particle size distribution of 40e63 mm and 230e400 ASTM. MS-ESI analyses were performed on Agilent 1100 LC/MSD trap system VL. All synthesized compounds were analyzed by CHN or by HPLC analysis performed on an Agilent 1260 Infinity instrument equipped with a 1260 DAD VLþ detector, and their purity is higher than 95%.

4.2. Materials

Tetrahydrofuran (THF) from a commercial source was purified by distillation (twice) from sodium wire under nitrogen. Dichloromethane from a commercial source was distilled from CaH_2 under nitrogen atmosphere before its use. Standardized

(2.50 M) n-butyllithium in hexane was purchased from Aldrich Chemical Co., and its titration was performed with N-pivaloyl-o-toluidine. Modified Micetich's procedure was used to prepare **1** (mofezolac) [8]; in particular, solid CO_2 was replaced by dry gaseous CO_2 and yields raised from 20 to 79%. 5-Aminopentanoic acid (**4**) and 11-aminoundecanoic acid (**5**) were purchased from Aldrich Chemical Co.. All other chemicals and solvents of commercial grade were further purified by distillation or crystallization prior to use.

4.3. Procedures for the preparation of galactopyranoside derivatives (2, 12 and 13)

The procedure to prepare **2** is described. **12** and **13** synthesis followed the same procedure used to obtain **2**. The exact amounts of reagents are reported in Table 5.

To a cold (ice-bath) solution of 2-(3,4-bis(4-methoxyphenyl) isoxazol-5-yl)acetic acid (**1**, mofezolac, 300 mg, 0.885 mmol) and 1,2:3,4-di-O-isopropylidene-D-galactose (230 mg, 0.885 mmol) in CH_2Cl_2 (5 mL), 4-(dimethylamino)pyridine (DMAP) (27 mg, 0.22 mmol), and N-(3-dimethylaminopropyl)-N^0-ethyl-carbodiimide hydrochloride (EDC HCl, 680 mg, 3.54 mmol) were added in small aliquots under argon atmosphere. The reaction mixture was stirred at room temperature for 24 h and then quenched by adding distilled water. The aqueous phase was extracted three times with EtOAc. The combined organic phases were dried over anhydrous Na_2SO_4, filtered, and the solvent removed under reduced pressure. The product (375 mg, 73% yield) was isolated by column chromatography (silica gel; $CHCl_3$/MeOH 95:5) of the reaction crude.

4.3.1. 1,2:3,4-Di-O-isopropylidene-6-O-{2-[3,4-bis(4-methoxyphenyl)isoxazol-5-yl]acetyl}-D-galactopyranose (2)

^{1}H NMR (300 MHz, $CDCl_3$, δ): 7.41–7.36 (m, 2H, aromatic protons); 7.19–7.14 (m, 2H, aromatic protons); 6.94–6.89 (m, 2H, aromatic protons); 6.85–6.81 (m, 2H, aromatic protons); 5.53 (d, 1H, J ¼ 4.9 Hz); 4.61 (dd,1H, J ¼ 8.0 Hz, J ¼ 2.5 Hz); 4.34–4.25 (m, 2H); 4.18 (dd, 2H, J ¼ 8.0 Hz, J ¼ 1.9 Hz); 4.05–3.99 (m, 1H); 3.83 (s, 3H, OCH_3); 3.80 (s, 3H, OCH_3); 3.79 (s, 2H, CH_2); 1.45 (s, 6H, $2CH_3$); 1.32 (s, 3H); 1.31 (s, 3H). ESI-MS m/z (%): $C_{31}H_{35}NO_{10}$ (M + Na)$^+$: 604.

4.3.2. 1,2:3,4-Di-O-isopropylidene-6-O-(5-{2-[3,4-bis(4-methoxyphenyl)isoxazol-5-yl]acetamido}pentanoyl)-D-galactopyranose (12)

Isolated 71 mg, 54% yield.^{1}H NMR (300 MHz, $CDCl_3$, δ): 7.33–7.31 (m, 2H, aromatic protons); 7.14–7.13 (m, 2H, aromatic protons); 6.86–6.85 (m, 2H, aromatic protons); 6.80–6.77 (m, 2H, aromatic protons); 6.43–6.41 (bs, 1H, NH: exchanges with D_2O), 5.49–5.47 (m, 1H); 4.57–4.55 (m, 1H); 4.29–4.23 (m, 3H); 4.18–4.12 (m, 2H); 3.99–3.97 (m, 1H); 3.86–3.66 (m, 1H); 3.77 (s, 3H, OCH_3); 3.73 (s, 3H, OCH_3); 3.61 (s, 2H, CH_2CONH); 3.26–3.22 (m, 1H, NHCHH); 3.21–3.15 (m, 1H, NHCHH); 2.32–2.30 (m, 2H, CH_2COO); 1.61–1.56 (m, 2H); 1.52–1.47 (m, 2H); 1.45 (s, 3H, CH_3); 1.39 (s, 3H, CH_3); 1.28 (s, 3H, CH_3); 1.27 (s, 3H, CH_3).^{13}C NMR (150 MHz, $CDCl_3$, δ): 173.1, 166.5, 162.7, 160.8, 160.3, 159.2, 130.9, 129.5, 121.3, 120.9, 117.2, 114.1, 113.7, 109.4, 108.6, 96.1, 77.2, 71.2, 70.8, 70.5, 70.4, 70.3, 70.2, 68.0, 65.9, 63.2, 61.9, 55.0, 54.9$_9$, 39.2, 33.7, 33.4, 28.3, 25.8, 25.7, 24.7, 24.2, 24.1, 21.9. ESI-MS: m/z (%): $C_{36}H_{44}N_2O_{11}$ (M + Na)$^+$: 703.

4.3.3. 1,2:3,4-Di-O-isopropylidene-6-O-(11-{2-[3,4-bis(4-methoxyphenyl)isoxazol-5-yl]acetamido}undecanoyl)-D-galactopyranose (13)

Isolated 95 mg, 25% yield.^{1}H NMR (300 MHz, $CDCl_3$, δ): 7.38–7.36 (m, 2H, aromatic protons); 7.15–7.14 (m, 2H, aromatic protons); 6.90–6.89 (m, 2H, aromatic protons); 6.84–6.82 (m, 2H, aromatic protons); 5.91–5.87 (bs, 1H, NH: exchanges with D_2O); 5.55 (d, 1H, J ¼ 5.0 Hz); 4.60 (dd, 1H, J ¼ 7.9 and 2.3 Hz); 4.32 (dd, 1H, J ¼ 5.0 and 2.3 Hz); 4.26 (dd, 1H, J ¼ 7.9 and 1.6 Hz); 4.25–4.13 (m,1H, CH); 3.90–3.80 (m, 2H, 2 CH); 3.81 (s, 3H, OCH_3); 3.79 (s, 3H, OCH_3); 3.64 (s, 2H, CH_2CONH); 3.23 (q, 2H, J ¼ 6.6 Hz, $NHCH_2$); 2.28 (t, 2H, J ¼ 7.6 Hz, CH_2COO); 1.62–1.54 (m, 2H); 1.48–1.42 (m, 2H); 1.52 (s, 3H, CH_3); 1.44 (s, 3H, CH_3); 1.32 (s, 3H, CH_3); 1.30–1.20 (m, 15H, $1CH_3$ and 6 CH_2).^{13}C NMR (150 MHz, $CDCl_3$, δ): 174.3, 166.4, 162.7, 161.1, 160.6, 159.5, 131.0, 129.7, 121.4, 121.0, 117.4, 114.4, 114.0, 109.4, 108.6, 96.3, 71.6, 70.7, 70.6, 68.1, 62.3, 55.24, 55.22, 51.4, 40.0, 34.2, 34.1, 29.4, 29.3, 29.2, 29.1, 26.8, 26.0, 25.9, 24.9, 24.3. ESI-MS m/z (%): $C_{42}H_{56}N_2O_{11}$ [M + H] : 763. ESI-MS-MS m/z (%): 503 (36), 294 (100), 264 (66). HRMS (ESI-TOF) m/z: [M + Na]$^+$ Calcd for $C_{42}H_{56}N_2O_{11}Na^+$ 787.3782; Found 787.3775.

4.4. Procedures for the preparation of 6 and 7

The procedure to synthesize **6** is described. **7** preparation followed the same procedure used to obtain **6**.

4.4.1. Methyl 5-aminopentanoate hydrochloride (6)

To a stirred solution 5-aminopentanoic acid (500 mg, 4.27 mmol) in anhydrous MeOH (5 mL) kept at 10 °C, $SOCl_2$ (1.1 mL, d ¼ 1.631 g/mL, 15 mmol) was dropwise added. The obtained reaction mixture was refluxed for 3 h. Then, excess $SOCl_2$ and MeOH were distilled under reduced pressure, using a NaOH trap. The product was obtained as a white solid in 79% yield (645 mg) and used in the following reaction without any further purification.^{1}H NMR (300 MHz, $CDCl_3$, δ): 8.35–8.28 (bs, 3H, $^+NH_3$: exchange with D_2O); 3.67 (s, 3H, OCH_3); 3.04 (m, 2H, CH_2NH_2); 2.38 (t, 2H, CH_2CO); 1.8–1.73 (m, 4H, CH_2CH_2).

4.4.2. Methyl 11-aminoundecanoate hydrochloride (7)

$SOCl_2$ (7.6 mmol),11-aminoundecanoic acid (2.49 mmol), MeOH (5 mL). The product was isolated as a white solid (535 mg, 86% yield).^{1}H NMR (300 MHz, $CDCl_3$, δ): 8.30–8.27 (bs, 3H, $^+NH_3$: exchange with D_2O); 3.64 (s, 3H, OCH_3); 2.90–2.85 (m, 2H, NH_2CH_2); 2.45–2.26 (m, 2H, CH_2CO); 1.71–1.56 (m, 2H, CH_2CH_2CO); 1.42–1.41 (m, 2H, $CH_2CH_2NH_2$); 1.36–1.18 (m, 12H, $6CH_2$).

4.5. Procedures for the preparation of derivatives 8 and 9

The procedure to synthesize **8** is described. **9** preparation followed the same procedure used to obtain **8**.

Table 5
Reagents amounts.

Main reagent(mol)[a]	1,2:3,4-Di-O-isopropylidene-D-galactose (mol)	DMAP (mol)	EDC (mol)
1 (0.885)	0.885	0.22	3.54
10 (0.194)	0.194	0.048	0.78
11 (0.5)	0.5	0.11	2

[a] 1, 10 and 11 were solubilized in CH_2Cl_2 (5 mL)

4.5.1. Methyl 5-{2-[3,4-bis(4-methoxyphenyl)isoxazol-5-yl] acetamido}pentanoate (8)

N-Diisopropyl-N-ethylamine (DIEA, 0.215 mL, 1.237 mmol) and methyl 5-aminopentanoate hydrochloride (6) (100 mg, 0.60 mmol) were solubilized in anhydrous CH_2Cl_2 (5 mL) and stirred at 0 C for 1 h. Then, this solution was dropwise added to a stirred solution of N,N^0 -dicyclohexylcarbodiimide (DCC, 170 mg, 0.825 mmol), 1-hydroxybenzotriazole monohydrate (HOBt H_2O, 180 mg, 1.05 mmol) and 2-[3,4-bis(4-methoxyphenyl)isoxazol-5-yl]acetic acid (mofezolac) (200 mg, 0.59 mmol) in anhydrous CH_2Cl_2 (20 mL) kept at 0 C. The reaction mixture was stirred for 19h at room temperature. Then, H_2O was added and the aqueous solution extracted with CH_2Cl_2. The combined organic layers were washed with a sat. aqueous solution of K_2CO_3, dried over anhydrous Na_2SO_4, and the solvent was removed under reduced pressure. Column chromatography of the crude residue (silica gel; EtOAc/ Hexane ¼ 3:7) allowed to isolated 8 (107 mg, 40% yield). FT-IR (KBr): 3458, 3089, 2987, 2948, 2849, 1737, 1652, 1609, 1562, 1516, 1455, 1441, 1426, 1253, 1233, 1175, 1108, 1029, 1019, 949, 831, 729 cm^{-1}.^{1}H NMR (300 MHz, $CDCl_3$, d): 7.41e7.37 (m, 2H, aromatic protons); 7.17e7.14 (m, 2H, aromatic protons); 6.92e6.89 (m, 4H, aromatic protons); 5.95e5.90 (bs, 1H, NH: exchanges with D_2O); 3.83 (s, 3H, OCH_3); 3.80 (s, 3H, OCH_3); 3.67 (s, 2H, CH_2COONH); 3.65 (s, 3H, OCH_3); 3.27 (q, 2H, J ¼ 6.9 Hz, $NHCH_2$); 2.33 (t, 2H, J ¼ 6.9 Hz, CH_2COO); 1.65e1.50 (m, 4H).^{13}C NMR (75 MHz, $CDCl_3$, d): 174.1, 166.8, 162.8, 161.4, 160.8, 159.7, 131.2, 130.0, 121.6, 121.2, 117.8, 114.6, 114.2, 55.5, 55.4, 39.7, 34.4, 33.6, 29.0, 22.2. ESI-MS: m/z (%): $C_{25}H_{28}N_2O_6$ (M þ Na)^þ: 475.

4.5.2. Methyl 11-{2-[3,4-bis(4-methoxyphenyl)isoxazol-5-yl] acetamido}undecanoate. (9)

Methyl 11-aminoundecanoate hydrochloride (1.38 mmol), DIEA (2.6 mmol), EDC HCl (1.58 mmol), HOBt H_2O (1.48 mmol), mofezolac (1.47 mmol), CH_2Cl_2 (48 mL)]. Column chromatography (silica gel; hexane/EtOAc ¼ 8:2) of the crude residue afforded the product as a white solid (573 mg, 72% yield).^{1}H NMR (300 MHz, $CDCl_3$, d): 7.41e7.26 (m, 2H, aromatic protons); 7.25e7.13 (m, 2H, aromatic protons); 6.93e6.71 (m, 4H, aromatic protons); 5.90e5.80 (bs, 1H, NH: exchanges with D_2O); 3.82 (s, 3H, OCH_3); 3.80 (s, 3H, OCH_3); 3.67 (s, 2H, CH_2); 3.65 (s, 3H, $COOCH_3$); 3.23e3.21 (m, 2H, $NHCH_2$); 2.31e2.26 (t, 2H, CH_2CO); 1.62e1.57 (m, 2H, CH_2CH_2CO); 1.49e1.45 (m, 2H, CH_2CH_2NH); 1.25e1.10 (m, 12H, 6 CH_2). ESI/MS m/z: $C_{31}H_{40}N_2O_6$ (Mþ Na)^þ: 559. HRMS (ESI-TOF) m/z: [Mþ Na]^þ Calcd for $C_{31}H_{40}N_2O_6Na^þ$: 559.2784. Found: 559.2781.

4.6. Procedures for the preparation of acid derivatives 10 and 11

The procedure to synthesize 10 is described. 11 preparation followed the same procedure used to obtain 10.

4.6.1. 5-{2-[3,4-Bis(4-methoxyphenyl)isoxazol-5-yl]acetamido} pentanoic acid (10)

To a solution of methyl 5-(2-(3,4-bis(4-methoxyphenyl)isoxazol-5-yl)acetamido)pentanoate (50 mg, 0.110 mmol) in THF (2 mL) was dropwise added a solution of 0.5 N LiOH (68 mg, 2.86 mmol, in 6 mL of H_2O) at room temperature. After 2 h,1 M HCl (5 mL) was added and the aqueous phase was extracted with EtOAc. The combined organic layers were dried over anhydrous Na_2SO_4 and the solvent evaporated under reduced pressure affording the product as a white solid (30 mg, 63% yield). FT-IR (KBr): 3330, 2921, 1720, 1641, 1607, 1540, 1514, 1468, 1424, 1406, 1303, 1247, 1180, 1030, 952, 901, 831 cm^{-1}.^{1}H NMR (300 MHz, $CDCl_3$, d): 7.37e7.34 (m, 2H, aromatic protons), 7.15e7.12 (m, 2H, aromatic protons); 6.90e6.87 (m, 2H, aromatic protons); 6.83e6.81 (m, 2H, aromatic protons); 6.35e6.28 (bs, 1H, NH: exchanges with D_2O); 3.81 (s, 3H, OCH_3); 3.78 (s, 3H, OCH_3); 3.67 (s, 2H, CH_2CONH); 3.26 (q, 2H, J ¼ 6.1 Hz, $NHCH_2$); 2.37 (t, 2H, J ¼ 6.6 Hz, CH_2COO); 1.61e1.41 (m, 4H, CH_2CH_2).^{13}C NMR (75 MHz, $CDCl_3$, d): 177.2, 166.9, 162.8, 161.4, 160.9, 159.7, 131.3, 130.1, 121.5, 121.1, 117.8, 114.6, 114.2, 55.6, 55.4, 39.7, 34.4, 33.3, 28.9, 21.9. ESI-MS: m/z (%): $C_{24}H_{26}N_2O_6$ [M-H]$^-$: 437.

4.6.2. 11-{2-[3,4-Bis(4-methoxyphenyl)isoxazole-5-yl]acetamido} undecanoic acid (11)

Methyl 11-{2-[3,4-bis(4-methoxyphenyl)isoxazol-5-yl]acetamido}undecanoate (9) (0.64 mmol), THF (10 mL), 0.5 M LiOH solution (36 mL). The product was obtained as a white powder (261 mg, 78% yield).^{1}H NMR (600 MHz, $CDCl_3$, d): 10.50e10.40 (bs, 1H, OH: exchanges with D_2O); 7.38 (d, 2H, J ¼ 8.7 Hz, aromatic protons); 7.15 (m, 2H, J ¼ 8.6 Hz, aromatic protons); 6.90 (d, 2H, J ¼ 8.6 Hz, aromatic protons); 6.83 (d, 2H, J ¼ 8.7 Hz, aromatic protons); 5.88 (bs, 1H, NH: exchanges with D_2O); 3.82 (s, 3H, OCH_3), 3.79 (s, 3H, OCH_3); 3.65 (s, 2H, CH_2CONH); 3.24 (q, 2H, J ¼ 6.6 Hz, $NHCH_2$); 2.28 (t, 2H, J ¼ 7.5 Hz, CH_2CO_2H); 1.62e1.56 (m, 4H, $CH_2CH_2CH_2CO_2H$); 1.47e1.44 (m, 2H, CH_2CH_2NH); 1.42e1.19 (m, 10H, 5 CH_2).^{13}C NMR (75 MHz, $CDCl_3$, d): 178.7, 174.1, 167.0, 166.8, 162.9, 161.3, 160.9, 159.7, 131.2, 130.0, 121.4, 121.0, 117.7, 114.6, 114.2, 55.6, 55.3, 40.3, 34.4, 34.0, 29.5, 29.4, 29.3, 29.2, 29.1, 26.9, 24.8. ESI-MS m/z (%): $C_{30}H_{38}N_2O_6$ [M-H] : 521. ESI-MS-MS m/z (%): 489 (4), 388 (50), 356 (54), 320 (100), 293 (9).

4.7. Procedure for the preparation of Galmofs (3, 14 and 15)

The procedure to synthesize 3 is described. 14 and 15 preparation followed the same procedure used to obtain 3.

4.7.1. 6-O-{2-[3,4-Bis(4-methoxyphenyl)isoxazol-5-yl]acetyl}-D-galactopyranose (3)

Trifluoracetic acid (TFA, 1.3 mL, d ¼ 1.47 g/mL, 16.7 mmol) was added to a solution of 1,2:3,4-di-O-isopropylidene-6-O-{2-[3,4-bis(4-methoxyphenyl)isoxazol-5-yl]acetyl}-D-galactopyranose (440 mg, 0.76 mmol) in anhydrous CH_2Cl_2 (5 mL). The progress of the reaction was monitored by TLC. The reaction mixture was stirred at room temperature for 24 h. Then, the solvent was distilled under reduced pressure and the product isolated as a white solid (148 mg, 39% yield) by a column chromatography (silica gel; $CHCl_3$/ MeOH ¼ 9:1) of the crude residue. M.p. 117e119 C.^{1}H NMR (500 MH_Z, $CDCl_3$, d): 7.29e7.27 (m, 2H, aromatic protons); 7.26e7.05 (m, 2H, aromatic protons); 6.81e6.80 (m, 2H, aromatic protons); 6.76e6.73 (m, 2H, aromatic protons); 5.50e5.35 (bs, 4H, OH: exchange with D_2O); 5.38 (s, 1H, 1^{0}H galactose); 4.60 (s, 1H, 3^{0}H galactose); 4.29e4.22 (m, 2H, 2^{0}H-4^{0}H galactose); 4.07e4.02 (m,1H, 5^{0}H galactose); 3.84e3.81 (dd, 2H, 6^{0}H galactose); 3.84 (s, 3H, OCH_3); 3.73 (s, 3H, OCH_3); 3.74 (s, 2H, OCH_2).^{13}C NMR (75 MHz, $CDCl_3$, d): 168.1, 161.9, 161.8, 160.7, 160.5, 159.3, 131, 129.7, 121.2, 120.8, 117.5, 114.3, 113.9, 72.4, 55.15, 31.6, 29.6. ESI-MS m/z (%): $C_{25}H_{27}NO_{10}$ (M þ Na)^þ: 524.

4.7.2. 6-O-(5-{2-[3,4-Bis(4-methoxyphenyl)isoxazol-5-yl] acetamido}pentanoyl)-D-galactopyranose (14)

[TFA (4 mmol), 12 (0.10 mmol), CH_2Cl_2 (2 mL)]. The product was isolated as a yellow solid (35 mg, 58%). M.p. 85e87 C. Anomeric ratio a/b ¼ 37/63.^{1}H NMR (500MH_Z, $CDCl_3$, d): 7.36e7.28 (m, 2H, aromatic protons); 7.20e7.18 (m, 2H, aromatic protons); 6.98e6.90 (m, 2H, aromatic protons); 6.90e6.84 (m, 2H, aromatic protons); 5.65e5.40 (bs, 5H, OH and NH: exchange with D_2O); 5.20e5.18 (m, 1^0-H, a anomer); 5.15e5.13 (m, 1^0-H, b anomer); 4.30e4.27 (m, 1H, 3^{0}H galactose); 4.10e4.09 (m, 2H, 2^{0}H-4^{0}H galactose); 3.85e3.83 (m, 2H, 6^{0}H galactose); 3.76 (s, 3H, OCH_3); 3.73 (s, 3H, OCH_3); 3.53e3.50 (m, 3H, CH_2CONH and 5^{0}H galactose); 3.07e3.01 (m, 2H, $NHCH_2$); 2.38e2.30 (m, 2H, CH_2CO_2); 1.5e1.38 (m, 4H, CH_2CH_2). ESI-MS m/z

(%): $C_{30}H_{36}N_2O_{11}$ [MþNa]^{þ}: 623.

4.7.3. 6-O-(11-{2-[3,4-Bis(4-methoxyphenyl)isoxazol-5-yl] acetamido}undecanoyl)-D-galactopyranose (15)

[TFA (8.72 mmol), 13 (0.226 mmol), CH_2Cl_2 (5 mL)]. The product was isolated as a white solid (70 mg, 45% yield) by a column chromatography (silica gel; $CHCl_3$/MeOH ¼ 9:1) of the crude residue. M.p. 88e90 C. Anomeric ratio a/b ¼ 30/70.^{1}H NMR (500 MHz, $CDCl_3$, d): 7.32e7.30 (m, 2H, aromatic protons); 7.13e7.11 (m, 2H, aromatic protons); 6.86e6.84 (m, 2H, aromatic protons); 6.80e6.78 (m, 2H, aromatic protons); 5.80-5.65 (bs, 4H, OH: exchange with D_2O); 5.20e5.17 (m, 1^0-H, a anomer); 5.15e5.14 (m, 1^0-H, b anomer); 4.71e4.53 (m, 1H, 3^0H); 4.24e4.19 (m, 2H, 2^0H and 4^0H); 4.09e3.96 (m, 2H, 6^0H); 3.78 (s, 3H, OCH_3); 3.76 (s, 3H, OCH_3); 3.61e3.53 (m, 4H, CH_2CONH and 5^0-H); 3.20e3.19 (m, 2H, NH_2CH_2); 3.0e2.34 (m, 2H, CH_2CO_2); 1.55e1.46 (m, 4H, $NHCH_2CH_2CH_2CH_2CO_2$); 1.26e1.11 (m, 12H, $CH_2(CH_2)_6CH_2$).^{13}C NMR (75 MHz, DMSO-d_6, d): 173.6, 166.8, 165.0, 160.8, 159.6, 131.6, 130.0, 122.0, 121.6, 117.0, 114.8, 73.7, 72.4, 55.8, 55.7, 34.0, 33.5, 29.6, 29.4, 29.1, 27.0, 25.1. ESI-MS m/z: $C_{36}H_{48}N_2O_{11}$: 707 [MþNa]^{þ}; ESI-MS-MS m/z: 689 (8), 647 (24), 584 (100), 545 (25). HRMS (ESI-TOF) m/z: [MþNa]^{þ} Calcd for $C_{36}H_{48}N_2O_{11}Na^{þ}$ 707.3156. Found 707.3154.

4.8. Cyclooxygenase activity inhibition determination

The target compounds were evaluated for their ability to inhibit ovine COX-1/COX-2 enzyme (percent inhibition at 50 mM). The inhibition of the enzyme was determined using a colorimetric COX inhibitor screening assay kit (Catalog No. 7601050, Cayman Chemicals, Ann Arbor, MI, USA) following the manufacturer's instructions. COX is a bifunctional enzyme exhibiting both cyclooxygenase and peroxidase activities. The cyclooxygenase component catalyzes the conversion of arachidonic acid into a hydroperoxide (PGG_2), and the peroxidase component catalyzes the reduction of endoperoxidase into the corresponding alcohol (PGH_2), the precursor of PGs, thromboxanes, and prostacyclin. The Colorimetric COX Inhibitor Screening Assay measures the peroxidase component of the cyclooxygenases. The peroxidase activity is assayed colorimetrically by monitoring the appearance of oxidized N,N,N^0 ,N^0 -tetramethyl-p-phenylenediamine (TMPD) at 590 nm. Stock solutions of test compounds were dissolved in a minimum volume of DMSO.

4.9. Permeability experiment

4.9.1. Preparation of Caco-2 monolayer

Caco-2 cells were harvested with trypsin EDTA and seeded onto a MultiScreen Caco-2 assay system at a density of 10,000 cells/well. The culture medium was replaced every 48 h for the first 6 days and every 24 h thereafter, and after 21 days in culture, the Caco-2 monolayer was utilized for the permeability experiments. The transepithelial electrical resistance (TEER) of the monolayers was measured daily before and after the experiment using an epithelial voltohmmeter (Millicell-ERS; Millipore, Billerica, MA). Generally, TEER values obtained are ~300 Ucm^2 for a 21 days culture [30].

4.9.2. Drug transport experiment

Apical to basolateral (Papp A/B) and basolateral to apical (Papp B/A) permeability of drugs was measured at 120 min at the concentration of 100 mM. Drugs were dissolved in Hank's balanced salt solution (HBSS, pH 7.4) and sterile filtered. After 21 days of cell growth, the medium was removed from filter wells and from the receiver plate. The filter wells were filled with 75 mL of fresh HBSS buffer, and the receiver plate, with 250 mL per well of the same buffer. This procedure was repeated twice, and the plates were incubated at 37 C for 30 min. For the experiments conducted in the presence of GLUT-1 inhibitor, cells were pre-incubated overnight with phloretin a 100 mM and then the normal protocol was followed.

After incubation, the HBSS buffer was removed, and, in some wells, drug solutions were added to the filter well (75 mL); HBSS without drug was added to the corresponding receiver plate (250 mL). For other wells, the drug solutions were added to the basolateral side (250 mL), and HBSS without drug was added to the corresponding filter wells. The plates were incubated at 37 C for 120 min. After incubation, samples were removed both from the apical (filter well) and basolateral (receiver plate) sides of the monolayer and then were stored in a freezer (20 C) till their analysis. The concentration of the compounds was analyzed by using UV VIS spectroscopy. The apparent permeability (Papp), in units of nm/sec, was calculated using the following equation:

$$Papp = \frac{VA}{(area \times time)} \times \frac{drug_{acceptor}}{drug_{initial}}$$

where VA is the volume (in mL) in the acceptor well, area is the surface area of the membrane (0.11 cm^2 of the well), time is the total transport time in seconds (7200 s), $[drug]_{acceptor}$ is the concentration of the drug measured by UV spectroscopy, and $[drug]_{initial}$ is the initial drug concentration (1 10^4 M) in the apical or basolateral well.

4.10. Immunofluorescence studies

Caco-2 cells were seeded at a density of 2500 cells per well in 96 well Collagen I-coated CellCarrier™ plate (Perkin-Elmer) and incubated for 18 h at 37 C and 5% CO_2.

Cells were rinsed in PBS and fixed with 4% formaldehyde for 30 min at room temperature. After PBS washes, fixed cells were incubated with BSA 3% to block non-specific antibody binding at r.t. for 20 min. Cells were then incubated overnight at 4 C with an anti-GLUT-1 mouse monoclonal antibody (dilution 1: 50; GLUT-1 (A-4): sc-377228, Santa Cruz Biotechnology, Inc.) or with BSA 3% (non-immune control). After several rinses with BSA 3%, cells were incubated with fluorescent donkey anti-mouse IgG antibody (dilution 1:400; Donkey anti-Mouse IgG (HþL) Secondary Antibody, Alexa Fluor® 594 conjugate, Thermo Fisher Scientific) for 1 h at r.t. in darkness.

Thereafter, cells were rinsed and counterstained with Hoechst 33342 (dilution:1 mg/mL) for 15 min at r.t. in darkness. Finally, after PBS washes,100 mL of PBS were dispensed and the plate was tightly sealed with sealing foil. The plate was then imaged on the Perkin-Elmer Operetta® High Content Screening system using the 20 long WD objective.

4.10.1. Competition experiments

To evaluate whether Galmofs are GLUT-1 substrates, a cell-based fluorescent competition assay was carried out using 2-deoxy-2-[(7-nitro-2,1,3-benzoxadiazol-4-yl)amino]-D-glucose (2-NBDG) (Molecular Probes, Inc. OR, USA), a fluorescently labeled GLUT-1 substrate as a fluorescent probe [31]. Confluent Caco-2 cells were washed with PBS for three times, and treated with the test solution of PBS containing Galmofs at different concentrations (0.01e0.1 mM) and 0.3 mM 2-NBDG for 10 min at 37 C in a humidified incubator (the 2-NBDG concentration was selected from preliminary experiments, reported in Supplementary material). Non-treated blank wells were used as the background, and D-glucose (0e10 mM) as the natural GLUT-1 substrate was used as positive control. 2-NBDG uptake was also inhibited

pharmacologically using the glucose uptake inhibitor phloretin (not shown). The reactions were stopped by adding ice-cold PBS, followed by three additional washes with PBS. All wells were then immediately imaged using a Perkin Elmer "Operetta" system equipped with a LWD 20 objective (Perkin Elmer, Inc. MA, USA). After the initial 2-NBDG imaging, nuclear labeling was performed by adding Hoechst 33342 ((Molecular Probes, Inc. OR, USA), 1 mM final concentration, dissolved in PBS and incubating for 10-min at 37 C. Images were acquired by the "Operetta" system, using a green channel filter set (465 nm_{ex}- 540 nm_{em}) for 2-NBDG, and a blue channel filter set (360 nm_{ex}- 420 nm_{em}) for Hoechst nuclear stain. Image acquisition and data analysis were performed by using the Harmony® Image Analysis Software (Perkin-Elmer, Inc. MA, USA). Automated analysis was performed to obtain as a readout the i) total number of cells (for information and quality control), ii) mean marker intensity (the marker intensity within the cell population), iii) the fraction of positive cells (the fraction of cells showing the marker), and iv) the mean marker intensity of positive cells. All raw values were normalized to control without 2-NBDG and presented as mean ± SEM of three independent experiments performed in triplicate.

4.11. PGE_2 assay

Mouse BV2 microglia cells (ICLC HTL 03001-Interlab Cell Line Collection) were grown in high glucose Dulbecco's modified Eagle's medium supplemented with 10% fetal bovine serum, 100 U/mL penicillin, and 100 mg/mL streptomycin. They were maintained at 37 C in a humidified 5% CO_2/95% environmental air. Mouse BV2 microglial cells were cultured in 6-well plates at a density of 3 10^6 cells/well. Then, the cells were pretreated with mofezolac (1) or $Galmof_0$ (3) for 1 h and, subsequently stimulated with LPS (1 mg/mL). Lipopolysaccharide from Escherichia coli serotype 0127: B8 was purchased from Sigma-Aldrich (Milan, Italy). The cultures were maintained at 37 C for 48 h in a humidified air containing a 5% CO_2. PGE_2 levels were determined in the supernatant using a competitive binding immunoassay (Cayman Chemical, Ann Arbor, MI, USA) following the manufacturer's instructions. Unstimulated cells were included as a control. The optical density was measured at l ¼ 415 nm with precision microplate reader and the amount of PGE_2 (ng/mL) was calculated using a PGE_2 standard curve.

4.12. HPLC analysis

Reversed-phase high-performance liquid chromatography (HPLC) was used to anlyze chemical and metabolic stability, and chromatographic purity of 3. The isocratic solvent system comprising of acetonitrile: 10 mM Tris-HCl pH 8 (15:85) was used as a mobile phase. The stationary phase was constituted by a Luna® 3 mm NH_2 100 Å, 250 4.6 mm Phenomenex® column that during the chromatographic runs was maintained at 40 C and $Galmof_0$ (3) was detected at 254 nm.

4.13. In vitro chemical stability of 3 ($Galmof_0$)

The chemical stability of 3 was determined in three different buffers simulating gastric fluid (pH 1; 0.1 M HCl), blood and gut district (respectively pH 7.3 and 8.0 [32]; 50 mM Tris-HCl) at 37 C. The reaction was initiated by adding 200 mL of stock solution of the compound (2.5 mg/mL) to 1,800 mL of the opportune buffer in a screw-capped glass vial. The solution was kept in a water bath at constant temperature, and samples (300 mL) were withdrawn at appropriate time intervals (15, 30, 60 min) diluted with 300 mL of acetonitrile, and analyzed by reverse HPLC. The percentage of prodrug remaining was calculated by using the following formula: % remaining ¼ (peak area at the respective time (min)/peak area at 0 min) x 100. (The elution profile of 3 is reported in the Supplementary material).

4.14. In vitro metabolic stability of 3 ($Galmof_0$) in rat liver S9 fraction

In vitro tests with rat liver S9 fraction (BD Bioscience, I-Milan) were designed as described by Jia and Liu with minor modifications [33]. 3 was incubated with rat liver S9 fraction (1 mg/mL) in 100 mM phosphate buffer (pH 7.4) containing 1.3 mM of $NADP^þ$, 3.3 mM glucose 6-phosphate and 0.4 U/mL glucose 6-phosphate dehydrogenase, and 3.3 mM $MgCl_2$ in a total volume of 1 mL. Incubations were commenced with the addition of glucose 6-phosphate dehydrogenase and carried out for 30 min at 37 C. The reaction was stopped by adding cool acetonitrile (1 mL). Immediately prior to add acetonitrile, samples were spiked with an internal standard. The samples were centrifuged at 4600 rpm for 15 min at 4 C. The supernatant was separated, and the acetonitrile phase was analyzed by HPLC. The percentage of the mean control concentration remaining after 30 min incubation was calculated according to the following equation:

$$\text{remaining substrate } (\%) \text{ after 30 min} = C_{parent} / C_{control} \times 100$$

where C_{parent} is ligand concentration after incubation with S9 fraction and NADPH regenerating system, and $C_{control}$ is ligand concentration after incubation with S9 fraction only.

4.15. Cell cycle progression

Caco-2 cells in exponential growth were cultured in plates of 10 cm^2 (150,000 cells/mL) in the absence of serum and at 37 C in a 5% CO_2 atmosphere. After 24 h in complete medium, the cells were exposed to a concentration of 100 mM of $Galmof_0$, $Galmof_5$, $Galmof_{11}$ and mofezolac for 24 h, while the control was incubated with vehicle (DMSO). At the end of the treatment, the adherent cells were washed, incubated with 0.2% trypsin for 5 min and harvested by centrifugation (1200 rpm,10 min). Cells were washed in PBS and fixed in 1 mL of ethanol at 70% ice. Samples containing 1 10^6 cells were centrifuged, rinsed in PBS, treated with 50 mg/mL RNase for 30 min at 37 C and then treated with 50 mg/mL propidium iodide (Sigma-Aldrich Chemie GmbH). The 10,000 cells were evaluated using a flow cytometer (Becton Dickinson Biosciences Pharmingen, USA) [34].

4.16. Computational methods

The computational tools employed in this work are mainly part of FLAP package. The in silico procedure began with the design of the Galmofs structures saved in minimized.mol2 format used in FLAP. Once the molecules were imported in FLAP, for each structure a maximum of 25 conformers were created, working at physiological pH conditions. FLAP was used in the structure-based mode and the template employed is the active site of the crystallographic structure: COX-1:mofezolac (PDB: 5HQK) [8]. The probes used in this analysis to generate the MIFs were the default probes DRY, O, N1 and H. It was, then, performed the "search for pockets" procedure, during which the system mimics the interactions between the default probes and the chemical environment of each amino acid present in the protein to recognize any active sites (protein pockets). The procedure was applied maintaining the default values (Number of additional trials ¼ 0, Sensitivity ¼ 6; Erosion ¼ 2) and without any constrains. FLAP compares the Molecular Interaction

Fields (MIFs) of the cavity to those of the test compounds ranking the poses according to a similarity score.

Funding sources

This work was supported by research funds through the University of Bari; MIUR (Rome - Italy) for Progetti di Ricerca Industriale nell'ambito del Programma Operativo Nazionale R&C 2007e2013 e Project "Research, Application, Innovation, Services in Bioimaging (R.A.I.SE.)" code PON01_03054; First AIRC Grant-MFAG2015 (Project Id. 17566).

Acknowledgment

The authors wish to thank Prof. Enza Lacivita (University of Bari) for her support in performing in vitro metabolic stability experiments.

Appendix A. Supplementary data

Supplementary data related to this article can be found at https://doi.org/10.1016/j.ejmech.2017.09.066.

References

[1] C.K. Glass, K. Saijo, B. Winner, M.C. Marchetto, F.H. Gage, Mechanisms underlying inflammation in neurodegeneration, Cell. 140 (2010) 918e934.

[2] L. Cartier, O. Hartley, M. Dubois-Dauphin, K. Krause, Chemokine receptors in the central nervous system: role in brain inflammation and neurodegenerative diseases, Brain Res. Brain Res. Rev. 48 (2005) 16e42.

[3] D. Kempuraj, R. Thangavel, P.A. Natteru, G.P. Selvakumar, D. Saeed, H. Zahoor, S. Zaheer, S.S. Iyer, A. Zaheer, Neuroinflammation induces neurodegeneration, J. Neurol. Neurosurg. Spine 1 (2016) 1e14.

[4] S.-H. Choi, S. Aid, F. Bosetti, The distinct roles of cyclooxygenase-1and -2 in neuroinflammation: implications for translational research, Trends Pharmacol. Sci. 30 (2009) 174e181.

[5] J.R. Barrio, N. Satyamurthy, S.-C. Huang, A.C. Petri, G.W. Small, V. Kepe, Dissecting molecular mechanisms in the living brain of dementia patients, Acc. Chem. Res. 42 (2009) 7842e7850.

[6] D. Melisi, A. Curcio, E. Luongo, E. Morelli, M.G. Rimoli, D-galactose as a vector for prodrug design, Curr. Top. Med. Chem. 11 (2011) 2288e2298.

[7] D.H. Rich, J. Green, M.V. Toth, G.R. Marshall, S.B. Kent, Hydroxyethylamine analogues of the p17/p24 substrate cleavage site are TightBinding inhibitors of HIV protease, J. Med. Chem. 33 (1990) 1285e1288.

[8] G. Cingolani, A. Panella, M.G. Perrone, P. Vitale, G. Di Mauro, C.G. Fortuna, R.S. Armen, S. Ferorelli, W.L. Smith, A. Scilimati, Structural basis for selective inhibition of Cyclooxygenase-1 (COX-1) by diarylisoxazoles mofezolac and 3-(5-chlorofuran-2-yl)-5-methyl-4-phenylisoxazole (P6), Eur. J. Med. Chem. 138 (2017) 661e668.

[9] R. Calvello, M.A. Panaro, M.L. Carbone, A. Cianciulli, M.G. Perrone, P. Vitale, P. Malerba, A. Scilimati, Novel selective COX-1 inhibitors suppress neuroinflammatory mediators in LPS-stimulated N13 microglial cells, Pharmacol. Res. 65 (2012) 137e148.

[10] R. Calvello, D.D. Lofrumento, M.G. Perrone, A. Cianciulli, R. Salvatore, P. Vitale, F. De Nuccio, L. Giannotti, G. Nicolardi, M.A. Panaro, A. Scilimati, Highly selective COX-1 inhibitors P6 and mofezolac counteract inflammatory state both in vitro and in vivo models of neuroinflammation, Front. Neurol 8 (2017) 1e10 (article 251).

[11] M.G. Perrone, P. Vitale, A. Panella, C.G. Fortuna, A. Scilimati, General role of the amino and methylsulfamoyl groups in selective cyclooxygenase(COX)-1 inhibition by 1,4-diaryl-1,2,3-triazoles and validation of a predictive pharmacometric PLS model, Eur. J. Med. Chem. 94 (2015) 252e264.

[12] P. Vitale, M.G. Perrone, P. Malerba, A. Lavecchia, A. Scilimati, Selective COX-1 inhibition as a target of theranostic novel diarylisoxazoles, Eur. J. Med. Chem. 74 (2014) 1e13.

[13] M.G. Perrone, P. Vitale, A. Panella, S. Ferorelli, M. Contino, A. Lavecchia, A. Scilimati, Isoxazole-based scaffold inhibitors targeting cyclooxygenase(COX)s, Chem. Med. Chem. 11 (2016) 1172e1187.

[14] P. Vitale, S. Tacconelli, M.G. Perrone, P. Malerba, L. Simone, A. Scilimati, A. Lavecchia, M. Dovizio, E. Marcantoni, A. Bruno, P. Patrignani, Synthesis, pharmacological characterization, and docking analysis of a novel family of diarylisoxazoles as highly selective cyclooxygenase-1 (COX-1) inhibitors, J. Med. Chem. 56 (2013) 4277e4299.

[15] Y. Yamamoto, J. Arai, T. Hisa, Y. Saito, T. Mukai, T. Ohshima, M. Maeda, F. Yamamoto, Isomeric iodinated analogs of nimesulide: synthesis, physicochemical characterization, cyclooxygenase-2 inhibitory activity, and transport across Caco-2 cells, Bioorg Med. Chem. 24 (2016) 3727e3733.

[16] J.E. Barnett, G.D. Holman, R.A. Chalkley, K.A. Munday, Evidence for two asymmetric conformational states in the human erythrocyte sugar-transport system, Biochem. J. 145 (1975) 417e429.

[17] A. Carruthers, J. DeZutter, A. Ganguly, S.U. Devaskar, Will the original glucose transporter isoform please stand up, Am. J. Physiol. Endocrinol. Metab. 297 (2009) 836e848.

[18] S. Agarwal, V. Arya, L. Zhang, Review of P-gp inhibition data in recently approved new drug applications: utility of the proposed [I(1)]/IC(50) and [I(2)]/IC(50) criteria in the P-gp decision tree, J. Clin. Pharmacol. 53 (2013) 228e233.

[19] D.S. Harris, J.W. Slot, H.J. Geuze, D.E. James, Polarized distribution of glucose transporter isoforms in Caco-2 cells, Acad. Sci. U. S. A. 89 (1992) 7556e7560.

[20] Z. Cheng, J. Levi, Z. Xiong, O. Gheysens, S. Keren, X. Chen, S. Sam Gambhir, Near-infrared fluorescent deoxyglucose analog for tumor optical imaging in cell culture and in living mice, Bioconjug. Chem. 17 (2006) 662e669.

[21] M. Hassanein, B. Weidow, E. Koeler, N. Bakane, S. Garbett, Y. Shyr, V. Quaranta, Development of high-throughput quantitative assays for glucose uptake in cancer cell lines, Mol. Imaging Biol. 13 (2011) 840e852.

[22] V. Barresi, C. Bonaccorso, G. Consiglio, L. Goracci, N. Musso, G. Musumarra, C. Satriano, C.G. Fortuna, Modeling, design and synthesis of new heteroaryl ethylenes active against the MCF-7 breast cancer cell-line, Mol. Biosyst. 9 (2013) 2426e2429.

[23] S. Sciabola, R.V. Stanton, J.E. Mills, M.M. Flocco, M. Baroni, G. Cruciani, F. Perruccio, J.S. Mason, High-throughput virtual screening of proteins using GRID molecular interaction fields, J. Chem. Inf. Model 50 (2010) 155e169.

[24] E. Carosati, G. Cruciani, A. Chiarini, R. Budriesi, P. Ioan, R. Spisani, D. Spinelli, B. Cosimelli, F. Fusi, M. Frosini, R. Matucci, F. Gasparrini, A. Ciogli, P.J. Stephens, F.J. Devlin, J. Med. Chem. 49 (2006) 5206e5216.

[25] G. Muratore, L. Goracci, B. Mercorelli, A. Foeglein, P. Digard, G. Cruciani, G. Palù, A. Loregian, Small molecule inhibitors of influenza A and B viruses that act by disrupting subunit interactions of the viral polymerase, PNAS 109 (2012) 6247e6252.

[26] S. Cross, M. Baroni, L. Goracci, G. Cruciani, GRID-based three-dimensional pharmacophores I: FLAPpharm, a novel approach for pharmacophore elucidation, J. Chem. Inf. Model 52 (2012) 2587e2598.

[27] S. Cross, F. Ortuso, M. Baroni, G. Costa, S. Distinto, F. Moraca, S. Alcaro, G. Cruciani, GRID-based three-dimensional pharmacophores II: PharmBench, a benchmark data set for evaluating pharmacophore elucidation methods, J. Chem. Inf. Model 52 (2012) 2599e2608.

[28] C.G. Fortuna, C. Bonaccorso, A. Bulbarelli, G. Caltabiano, L. Rizzi, L. Goracci, G. Musumarra, A. Pace, A. Palumbo-Piccionello, A. Guarcello, P. Pierro, C.E. Cocuzza, R. Musumeci, New Linezolid-like 1,2,4-oxadiazoles active against Gram-positive multiresistant pathogens, Eur. J. Med. Chem. 65 (2013) 533e545.

[29] S. Cross, M. Baroni, E. Carosati, P. Benedetti, S. Clementi, FLAP: GRID molecular interaction fields in virtual screening. validation using the DUD data set, J. Chem. Inf. Model. 50 (2010) 1442e1450.

[30] B. Srinivasan, A.R. Kolli, M.B. Esch, H.E. Abaci, M.L. Shuler, J.J. Hickman, TEER measurement techniques for in vitro barrier model systems, J. Lab. Autom. 20 (2015) 107e126.

[31] K. Yamada, M. Saito, H. Matsuoka, A real-time method of imaging glucose uptake in single, living mammalian cells, Nat. Protoc. 2 (2007) 753e763.

[32] A. Curcio, O. Sasso, D. Melisi, M. Nieddu, G. La Rana, R. Russo, E. Gavini, G. Boatto, E. Abignente, A. Calignano, M.G. Rimoli, Galactosyl prodrug of ketorolac: synthesis, stability, and pharmacological and pharmacokinetic evaluations, J. Med. Chem. 25 (2009) 3794e3800.

[33] L. Jia, X. Liu, The conduct of drug metabolism studies considered good practice (II): in vitro experiments, Curr. Drug Metab. 8 (2007) 822e829.

[34] Z. Darzynkiewicz, H.A. Crissman, J.P. Robinson, Methods in cell biology, Cytometry 41 (1994) 351e376.